

AN EFFICIENT SEMI-ANALYTICAL FINITE FRACTURE MECHANICS APPROACH FOR THE PREDICTION OF INTERLAMINAR CRACK INITIATION IN COMPOSITE LAMINATES

S. DÖLLING, S. HELL AND W. BECKER

Technische Universität Darmstadt, Fachgebiet Strukturmechanik,
Franziska-Braun-Straße 7,
D-64287 Darmstadt, Germany
{doelling, hell, becker}@fsm.tu-darmstadt.de
www.fsm.tu-darmstadt.de

Key words: laminate free-edge effect, scaled boundary finite element method, finite fracture mechanics

Abstract. The discontinuous stiffness properties of composite laminates theoretically induce infinite stresses at free edges. These highly localized interlaminar stresses may lead to a premature failure of the laminate. Due to infinite stresses and the absence of a pre-existing crack, neither classical strength-based nor purely energy-based failure criteria allow for reliable failure load predictions. These drawbacks are overcome by the coupled stress and energy criterion within the framework of finite fracture mechanics (FFM). This approach has already proven successful for the analysis of interlaminar crack initiation in angle-ply laminates. However, the analyses based on the finite element method typically go along with a high numerical effort. In the present study, interlaminar crack initiation at a free edge in symmetric laminates based on a generalized plane strain model is investigated using FFM. Initially, the problem is again treated using the finite element method acting as a reference solution. But compared to former works interface fracture properties are not determined through a parameter fit. Instead, realistic interface fracture properties are taken into account yielding a good agreement with experiments from literature. The goal of the present work is to predict interlaminar crack onset in composite laminates using FFM in combination with the highly efficient semi-analytical scaled boundary finite element method (SBFEM) which significantly reduces the numerical effort compared to the FEM. First results show the high potential of the SBFEM in comparison with the FEM.

1 Introduction

Since the late sixties the existence of interlaminar stresses on the interface between two dissimilar layers along composite laminates' free edges, with probably negative impact on the effective strength, is known [1]. In 1970 Pipes and Pagano [2] investigated the interlaminar shear stress distribution in symmetric four-layer angle-ply laminates subjected to axial loads. Their results revealed the singular nature of the interlaminar shear and normal stresses at the free edge caused by the discontinuous stiffness properties of the layers. Subsequently, the pioneering work of Pipes and Pagano triggered many studies examining the free-edge effect. Thereby, the

investigations focused on the three-dimensional singular stress field at the free edge. For an overview, the reader is referred to [3, 4]. Beyond that, the investigation of the local stress field and its influence upon laminate strength was a crucial issue. In 1974, Whitney and Nuismer [5] proposed the evaluation of a stress criterion averaged over a certain distance, the so called critical length, in order to tackle stress concentrations in laminates. The critical length was assumed to be a material property and independent of laminate layup. Alternatively, several fracture mechanics approaches were employed [6, 7]. However, due to the lack of a pre-existing crack an assumption regarding a critical length or inherent flaw size was still needed.

In order to avoid the use of a critical length, which is not a material parameter and depends on the structural situation and load [8, 9, 10], Leguillon [11] introduced a coupled stress and energy criterion within the framework of finite fracture mechanics (FFM). This criterion allows for the prediction of crack initiation in terms of the arising crack length as well as the corresponding failure load. An overview can be found in Weißgraeber et al. [12]. A FFM approach has been applied by Martin et al. [13] for the prediction of interlaminar crack onset induced by the free-edge effect in symmetric angle-ply laminates according to the Pipes and Pagano model. The required field quantities were determined by means of finite element method. A strong mesh refinement towards the interface is needed due to the singular character of the stress field at the free edge leading to a high numerical effort.

In the present study, interlaminar crack initiation at a free edge in selected symmetric angle-ply laminates is investigated in the framework of FFM. First, the problem is treated by the finite element method according to Martin et al. to get a reference solution. Differing from Martin et al. no interface fracture properties fit is performed. Instead, the interface fracture properties are determined based on the matrix resin properties. The results obtained by the finite element method are in good agreement to experimental findings by Lagunegrad et al. [14] considering physically reasonable interface fracture properties. Second, the numerical effort is significantly reduced using the semi-analytical scaled boundary finite element method (SBFEM) to determine the required singular stress fields. The SBFEM was originally developed by Song and Wolf [15] for elastodynamics soil-structure interaction problems typically involving large and boundless domains. Later, the method has been successfully applied to a wide range of problems governed by linear partial differential equations, for instance, to predict crack initiation in different structural situations using FFM [16]. The SBFEM reduces the dimension of the problem by one due to a suitable product ansatz attended by a coordinate transformation. In the current case only the boundary has to be discretized by one-dimensional finite elements. The former governing partial differential equations are reduced to ordinary differential equations. The coefficients of the simplified differential equations are determined by the finite element method performed on the boundary. Finally, the ordinary differential equations are solved. The application of the SBFEM to the free-edge effect is still subject of current research.

2 Modeling

The physical model addressing the free-edge effect is conducted according to Pipes and Pagano [2]. Only symmetric angle-ply laminates, consisting of four unidirectional layers, are considered. The fiber direction is given by the angle ϑ with respect to the global x, y, z -laminate coordinate system as depicted in Figure 1. The material coordinate system of each layer i is denoted by x_1^i, x_2^i, x_3^i . The single layer is supposed to be homogeneous and orthotropic. Linear elastic material behavior is assumed. The validity of Saint-Venant's Principle is postulated such

that local effects induced by load introduction are negligible at sufficiently large distances. The laminate is subjected to a uniform axial extension load ε_0 at its ends. Hence, stresses and strains are independent of x . Under the mentioned conditions the displacement field with respect to the global laminate coordinate system is assumed to be

$$u(x, y, z) = \varepsilon_0 \cdot x + \tilde{u}(y, z), \quad v(x, y, z) = \tilde{v}(y, z) \quad w(x, y, z) = \tilde{w}(y, z). \quad (1)$$

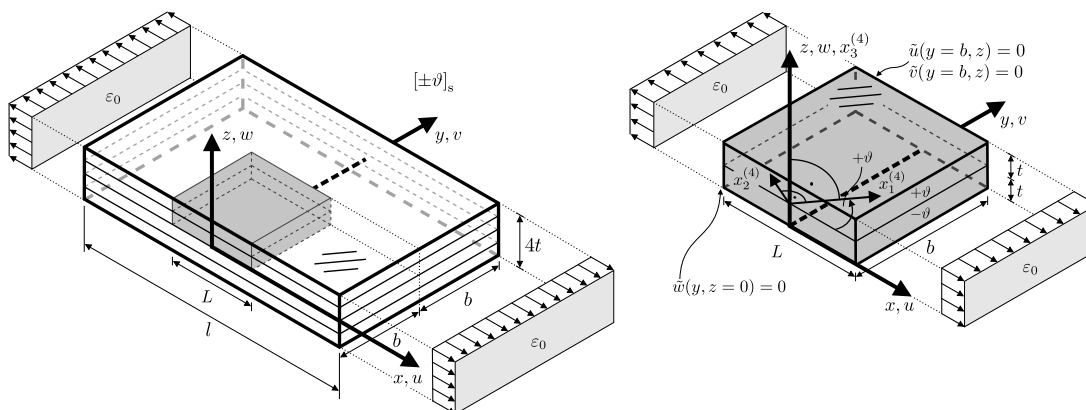


Figure 1: *Left*: Part of a four layer symmetric angle-ply laminate subjected to a uniaxial extension load ε_0 . *Right*: View of the deduced quarter model.

Differentiating the first equation with respect to x shows that the axial strain $\varepsilon_{xx} = \varepsilon_0$ is constant within the whole laminate. This state is called generalized plane strain state. Combining the classical equations of elasticity with respect to the assumed displacement field (1) yields a set of coupled, second-order partial differential equations for the unknown displacement field. The $[\pm\vartheta]_S$ laminate model can be simplified as a quarter model with respect to the x - y -symmetry plane intersecting the laminate coordinate system origin and a x - z -plane of symmetry at $y = b$ as depicted right in Figure 1. The corresponding symmetry boundary conditions are given by

$$\tilde{w}(y, z = 0) = 0, \quad \tilde{u}(y = b, z) = 0, \quad \tilde{v}(y = b, z) = 0. \quad (2)$$

In order to validate the predicted failure loads related to interlaminar crack onset the experiments of Lagunegrad et al. [14] are taken into account. The thickness of a single ply as well as the elasticity properties are taken from Lagunegrad et al. and can be found in Table 1. The laminate width is set to $b = 10$ mm. The length L is arbitrarily chosen to 0.05 mm. According to the generalized plane strain state, the chosen length L has no impact to the stresses and strains.

Table 1: Properties of a single ply with respect to the material coordinate system for the G947/M18 laminate [14].

E_{11} [GPa]	E_{22} [GPa]	E_{33} [GPa]	G_{12} [GPa]	G_{13} [GPa]	G_{23} [GPa]	ν_{12}	ν_{13}	ν_{23}	t [mm]
97.6	8.0	8.0	3.1	3.1	2.7	0.37	0.37	0.5	0.19

3 Finite fracture mechanics

Due to the weak singular stress field and the lack of a pre-existing crack neither classical stress based criteria, nor fracture mechanics approaches allow for a prediction of failure loads for interface crack onset at laminates' free edges. The singular stress field leads to an automatic fulfillment of stress based criteria. Linear elastic fracture mechanics (LEFM) approaches are restricted to crack-like singularities. In order to overcome the limitation of LEFM based energy criteria the incremental energy release rate $\bar{\mathcal{G}}$ was introduced.

$$\bar{\mathcal{G}} = \frac{1}{\Delta A} \int_0^{\Delta A} \mathcal{G}(\tilde{A}) d\tilde{A} = -\frac{\Delta \Pi}{\Delta A}, \quad (3)$$

where \mathcal{G} denotes the differential energy release rate, A the crack area and Π the total energy potential. Note that Eq. (3) is not restricted to crack singularities. By means of the incremental energy release rate a Griffith-type criterion can be formulated. As a consequence, the unknown finite crack size ΔA has to be determined in addition to the unknown failure load P_f . Leguillon [11] proposed a coupled stress and energy based criterion in order to determine the failure load as well as the finite crack size. In general, the coupled criterion can be given as

$$f(\boldsymbol{\sigma}(\mathbf{x}, P)) \geq \sigma_c \quad \forall \mathbf{x} \in \Omega_c(\Delta A) \quad \wedge \quad \bar{\mathcal{G}}(\Delta A, P) \geq \mathcal{G}_c, \quad (4)$$

where Ω_c denotes the potential crack surface. Regarding the given symmetric four-layer angle-ply laminate solely crack initiation in the interface between the $+\vartheta$ and the $-\vartheta$ layer induced by free-edge effect is investigated. The simultaneous appearance of four similar cracks, each starting from the free edge of an intersection between differently orientated layers, is assumed. As shown subsequently, interlaminar stresses as well as the incremental energy release rate behave strictly monotonic in the vicinity of the free edge. Hence, the coupled criterion (4) can be formulated by means of equalities instead of inequalities. In the present work, only angle-ply laminates up to $[\pm 30^\circ]_S$ are investigated such that the interlaminar stresses σ_{xz} are predominant in the interface in the vicinity of the free edge. Thus, according to Martin et al., a simple stress criterion is chosen accounting for σ_{xz} along the interface only. The crack size can be expressed as $\Delta A = L \cdot \Delta a$ in which L denotes the length of the model (Figure 1) and Δa the crack length in y -direction. The coupled criterion for the investigated structural situation is given by

$$\sigma_{xz} \left(y = \Delta a_c, \varepsilon_0 = \varepsilon_0^f \right) = \sigma_{xz} \left(\Delta a_c, \varepsilon_0^* \right) \frac{\varepsilon_0^f}{\varepsilon_0^*} = \tau_c, \quad (5)$$

$$\bar{\mathcal{G}} \left(\Delta a = \Delta a_c, \varepsilon_0 = \varepsilon_0^f \right) = \bar{\mathcal{G}} \left(\Delta a_c, \varepsilon_0^* \right) \left(\frac{\varepsilon_0^f}{\varepsilon_0^*} \right)^2 = \mathcal{G}_{3c} = \mathcal{G}_c, \quad (6)$$

where Δa_c denotes the unknown crack length and ε_0^f the unknown failure strain. In this particular case, the interlaminar stress behavior as well as the incremental energy release rate is determined only once for the arbitrarily chosen load $\varepsilon_0^* = 1$ and scaled to any load for a fixed laminate layup. Combining Eq. (5) and Eq. (6) yields

$$\frac{\bar{\mathcal{G}}(\Delta a_c, \varepsilon_0^*)}{(\sigma_{xz}(\Delta a_c, \varepsilon_0^*))^2} = \frac{\mathcal{G}_c}{\tau_c^2}. \quad (7)$$

Determination of the roots of Eq. (7) provides the sought critical crack length Δa_c . Furthermore, it can be seen that the length of an initiated interface crack solely depends on the interface fracture toughness \mathcal{G}_c and strength τ_c . Substituting the obtained critical crack length either into Eq. (5) or Eq. (6) gives the corresponding failure strain ε_0^f .

4 Finite element reference model

The finite element method is used to obtain a reference solution for the introduced problem. To this end, the quarter model (Figure 1) has been implemented in the commercial FE software *Abaqus*. A consistent implementation with respect to Pipes and Pagano’s work is realized using only one element in x -direction. To satisfy the assumed generalized plane strain state, degrees of freedom of opposite nodes in the x -direction are coupled by means of multi-point constraints. In order to capture the laminate free-edge effect properly, the mesh is refined towards the interface as well as the free edge. A convergence study has been performed to ensure an accurate evaluation of the interface stresses and incremental energy release rates. The smallest element size found at the bi-material point of the free edge, is about 0.001 mm. Due to the refinement the model in total includes about 143000 degrees of freedom. Fully integrated three-dimensional brick elements with quadratic shape functions have been used (C3D20).

5 Results obtained by the finite element method

In this section results of the finite element analyses are presented and compared to experimental data from literature. Crack initiation is expected in the interface between the $+\vartheta$ and $-\vartheta$ layer. Hence, stresses along this interface are investigated. The obtained interface stresses are depicted in Figure 2a-c. The interlaminar shear stress σ_{xz} as well as the normal stress σ_{zz} becomes singular at the free edge. In order to meet the boundary condition at the free edge, the interlaminar shear stress σ_{yz} decays to zero. As mentioned before, the interface shear stress σ_{xz} is predominant in the vicinity of the free edge for the considered laminate layups so that this stress is accounted for evaluation of the stress criterion solely. Note, that the predominant σ_{xz} shear stress rapidly decays towards the interior laminate so that it vanishes in a distance of about three times the single ply thickness t . In comparison, the interlaminar stress σ_{zz} as well as the shear stress σ_{yz} fade out slower. They subside after about six and eight times the single-ply thickness. The incremental energy release rate $\bar{\mathcal{G}}$ is evaluated with respect to potential interface cracks of the length Δa (Figure 2d) using

$$\bar{\mathcal{G}}(\varepsilon_0^*, \Delta a) = -\frac{W(\varepsilon_0^*, \Delta a) - W(\varepsilon_0^*, \Delta a = 0)}{\Delta a L}. \quad (8)$$

W denotes the elastic strain energy of the arbitrarily loaded laminate quarter model. As depicted, the incremental energy release rate reaches a plateau for longer cracks. In consideration of Eq. (8) Equation (7) yields the critical crack length Δa_c with respect to the quotient of interface fracture properties as shown in Figure 3a. In order to be able to evaluate failure loads for the investigated laminates, the actual interface fracture properties must be known a priori. The determination of interface fracture properties has been widely discussed in literature. However, it can be summarized that it is difficult to measure them. Due to the lack of reliable interface fracture properties for the investigated G947/M18 angle-ply laminates the following assumptions are made. As a first approximation, it is presumed that the interface fracture properties are dominated by the properties of the epoxy matrix resin (Table 2).

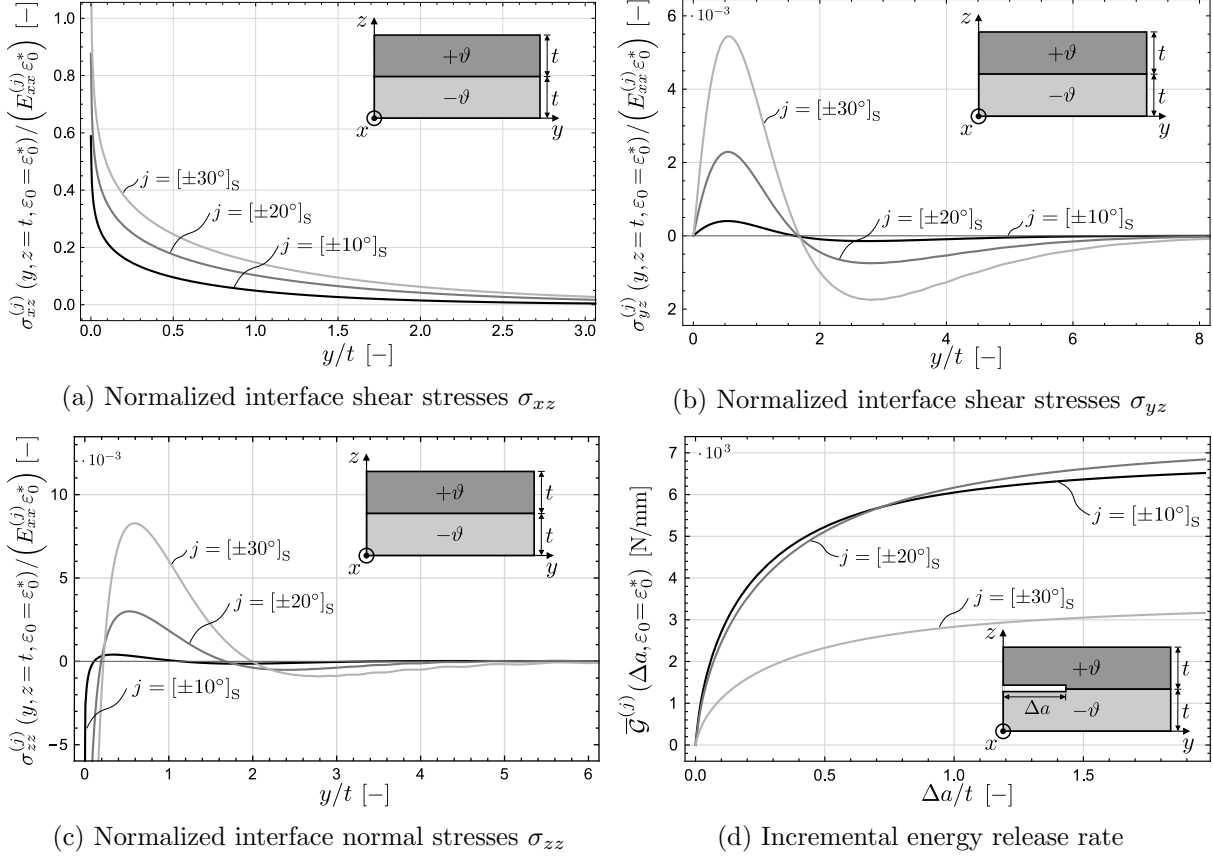


Figure 2: Normalized interface stresses and incremental energy release rates for selected G947/M18 angle-ply laminates, obtained by the finite element method. The interface stresses are normalized with respect to the particular effective laminate stiffness E_{xx} . The effective stiffness is determined based on CLPT such that $E_{xx} = \frac{1}{4t} \left(A_{11} - \frac{A_{12}^2}{A_{22}} \right)$, in which A_{ij} denotes the extensional stiffness quadrant of the laminate stiffness matrix.

Table 2: Properties of the cured (180°C) M18 matrix resin according to the manufacturer [17].

E [GPa]	ν	R_{σ}^m [MPa]	\mathcal{G}_{Ic}^m [N/mm]
3.5	0.38	81.1	0.193

Consequently, and based on [18], it is assumed that the laminate's mode 1 interface fracture toughness \mathcal{G}_{1c} is about the matrix fracture toughness \mathcal{G}_{Ic}^m . In literature, mode 1 interface fracture toughnesses for composites are within a range of 0.08 - 1.0 N/mm [18, 19]. Furthermore, the mode 3 interface fracture toughness is set to $\mathcal{G}_{3c} = 2\mathcal{G}_{1c}$. As shown in Figure 2a-c the interlaminar shear stresses σ_{xz} are predominant. Hence, the critical interface strength is set to $\tau_c = R_{\sigma}^m / \sqrt{3}$ according to the von Mises criterion. Based on the solution of Eq. (7) the corresponding failure strains, with respect to the interface fracture properties, are obtained using Eq. (6), and depicted in Figure 3b-d. The failure strain predictions for the chosen interface fracture properties can be found in Table 3 in comparison to experimental findings from literature. The predicted results slightly underestimate the experiments. However, the differences are within an error range of 8.83% and 2.63% only.

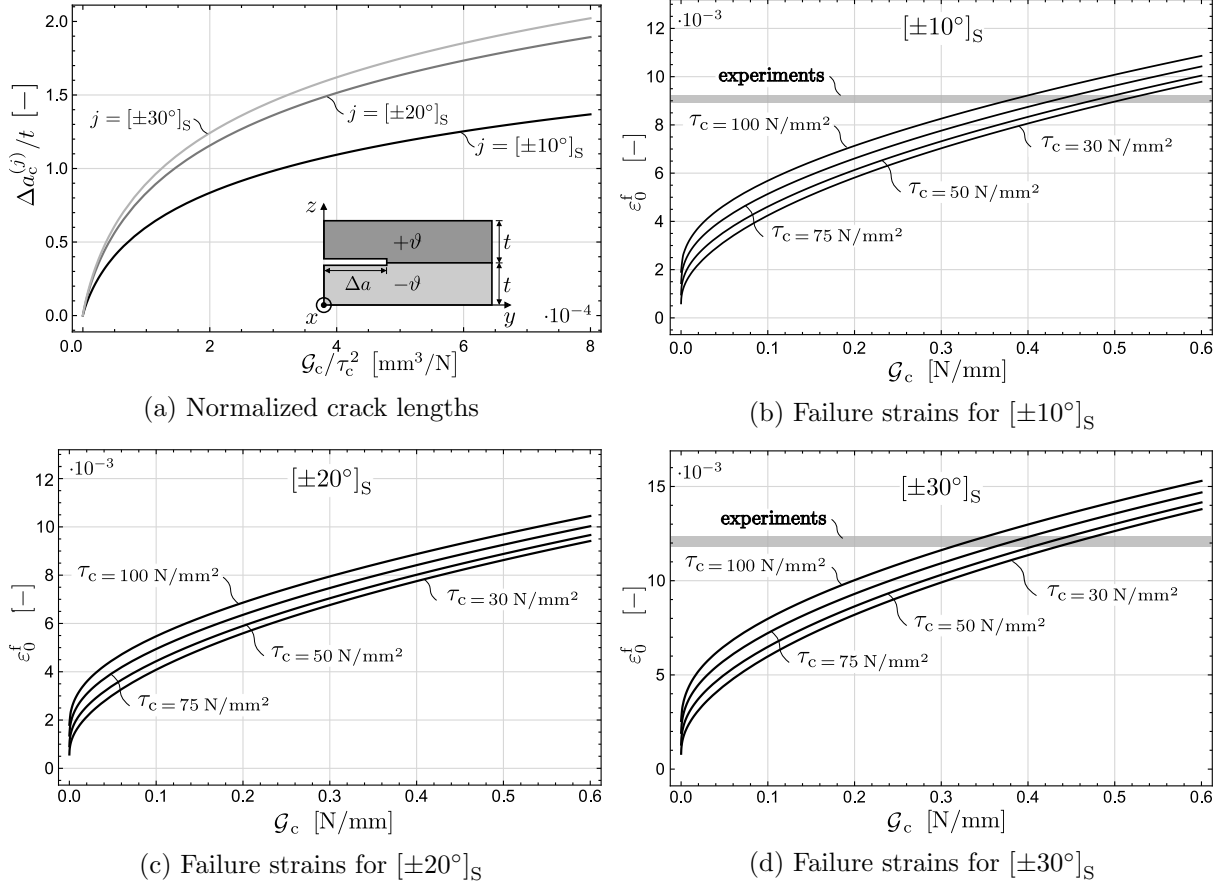


Figure 3: Predicted normalized crack lengths and corresponding failure strains with respect to the interface fracture properties \mathcal{G}_c and τ_c for selected G947/M18 angle-ply laminates. For comparison, the failure strains experimentally determined by [14] are also shown.

Table 3: Predicted failure strains ε_0^f with respect to the chosen interface fracture properties in comparison to the experimentally determined failure strains $\varepsilon_{0,\text{exp}}^f$ by Lagunegrand et al. [14].

layup	τ_c [MPa]	\mathcal{G}_c [N/mm]	$\Delta a_c/t$ [-]	ε_0^f [-]	$\varepsilon_{0,\text{exp}}^f$ [-]
$[\pm 10^\circ]_S$	47.2	0.386	0.784	0.00816	0.00895 – 0.00917
$[\pm 20^\circ]_S$	47.2	0.386	1.086	0.00785	–
$[\pm 30^\circ]_S$	47.2	0.386	1.167	0.01149	0.01180 – 0.01230

6 Scaled Boundary Finite Element Method

In the following, the scaled boundary finite element is introduced. The considered domain has to fulfill the geometrical scaling requirement. The investigated structural situation has to be a star domain. The scaling center S lies on the free edge at the interface between the $+\vartheta$ and $-\vartheta$ layer (Figure 4). A scaled boundary ξ, η -coordinate system is introduced. The scaled radial ξ -coordinate starts at the scaling center where it takes the value zero and reaches the value 1 on the boundary. A part of the boundary Γ_d (red marked) is characterized by the boundary coordinate η . Any point which is part of the domain is described by scaling the corresponding point on the boundary Γ_d with ξ . The transformation from the Cartesian x, y, z -coordinate

system into scaled boundary ξ, η -coordinate system is described by

$$\mathbf{x} = \mathbf{x}_S + \xi \mathbf{x}_\eta(\eta), \quad (9)$$

where \mathbf{x}_S denotes the Cartesian coordinates of the scaling center.

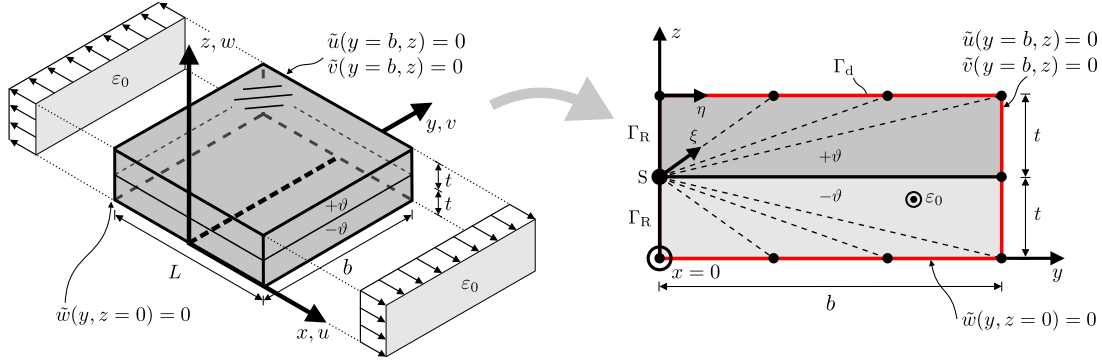


Figure 4: SBFEM quarter model for the four-layer angle-ply laminate.

The corresponding Jacobian matrix $\mathbf{J}_\eta(\eta)$, only depending on the boundary coordinate η , is given by

$$\begin{bmatrix} \frac{\partial}{\partial \xi} \\ \frac{\partial}{\partial \eta} \end{bmatrix} = \begin{bmatrix} \frac{\partial y(\xi, \eta)}{\partial \xi} & \frac{\partial z(\xi, \eta)}{\partial \xi} \\ \frac{\partial y(\xi, \eta)}{\xi \partial \eta} & \frac{\partial z(\xi, \eta)}{\xi \partial \eta} \end{bmatrix} \begin{bmatrix} \frac{\partial}{\partial y} \\ \frac{\partial}{\partial z} \end{bmatrix} = \mathbf{J}_\eta(\eta) \begin{bmatrix} \frac{\partial}{\partial y} \\ \frac{\partial}{\partial z} \end{bmatrix} \quad (10)$$

The transformation of the derivatives can be performed using the differential operator \mathcal{L} to

$$\mathcal{L} = \begin{bmatrix} 0 & 0 & 0 \\ 0 & 1 & 0 \\ 0 & 0 & 0 \\ 0 & 0 & 1 \\ 0 & 0 & 0 \\ 0 & 0 & 0 \\ 1 & 0 & 0 \end{bmatrix} \frac{\partial}{\partial y} + \begin{bmatrix} 0 & 0 & 0 \\ 0 & 0 & 0 \\ 0 & 0 & 1 \\ 0 & 1 & 0 \\ 1 & 0 & 0 \\ 0 & 0 & 0 \end{bmatrix} \frac{\partial}{\partial z} = \mathbf{L}_y \frac{\partial}{\partial y} + \mathbf{L}_z \frac{\partial}{\partial z} = \mathbf{L}_\xi \frac{\partial}{\partial \xi} + \mathbf{L}_\eta \frac{1}{\xi} \frac{\partial}{\partial \eta}, \quad (11)$$

where \mathbf{L}_ξ and \mathbf{L}_η are given by

$$\mathbf{L}_\xi = \mathbf{L}_y j_{11} + \mathbf{L}_z j_{21}, \quad \mathbf{L}_\eta = \mathbf{L}_y j_{12} + \mathbf{L}_z j_{22},$$

and j_{mn} ($m, n = 1, 2$) denotes the components of the inverse Jacobian matrix \mathbf{J}_η^{-1} . The transformed differentials are described by

$$dV = \det(\mathbf{J}_\eta) \xi d\eta d\xi, \quad dA = \left\| \frac{\partial \mathbf{x}_\eta}{\partial \eta} \right\| \xi d\eta.$$

A finite element method is performed on a part of the boundary Γ_d (Figure 4) under the assumption of a separation ansatz in order to determine the unknown displacements $\tilde{u}, \tilde{v}, \tilde{w}$ with respect to the ξ, η -coordinate system. The separation of variables ansatz is given by

$$\mathbf{u}(\xi, \eta) \approx \tilde{\mathbf{u}}(\xi, \eta) = \mathbf{N}(\eta) \hat{\mathbf{u}}(\xi). \quad (12)$$

in which the matrix of piecewise polynomial shape functions only depending of the boundary coordinate η is denoted with $\mathbf{N}(\eta)$. The unknown free values $\hat{\mathbf{u}}(\xi)$ are scaled with ξ such that

the nodal displacements on the boundary are described for $\xi = 1$. The corresponding strains are given by

$$\tilde{\boldsymbol{\varepsilon}}(\xi, \eta) = \mathcal{L}\tilde{\mathbf{u}} + \mathbf{S} = \mathbf{B}_\xi \hat{\mathbf{u}}_{,\xi} + \mathbf{B}_\eta \frac{1}{\xi} \hat{\mathbf{u}} + \mathbf{S}, \quad (13)$$

in which \mathbf{S} describes the extension load ε_0 and

$$\mathbf{B}_\xi = \mathbf{L}_\xi \mathbf{N}(\eta), \quad \mathbf{B}_\eta = \mathbf{L}_\eta \mathbf{N}_{,\eta}(\eta).$$

Using the principle of virtual displacements, with vanishing stresses tractions on boundary and vanishing volume loads, yields the SBFEM basic equations

$$\xi^2 \mathbf{K}_0 \hat{\mathbf{u}}_{,\xi\xi}(\xi) + \xi (\mathbf{K}_0 + \mathbf{K}_1^\text{T} - \mathbf{K}_1) \hat{\mathbf{u}}_{,\xi}(\xi) - \mathbf{K}_2 \hat{\mathbf{u}}(\xi) + \xi (\mathbf{S}_\xi - \mathbf{S}_\eta) = \mathbf{0}, \quad (14)$$

$$\mathbf{K}_0 \hat{\mathbf{u}}_{,\xi}(\xi = 1) + \mathbf{K}_1^\text{T} \hat{\mathbf{u}}(\xi = 1) + \mathbf{S}_\xi = \mathbf{0}, \quad (15)$$

$$\mathbf{K}_1^\text{T} \hat{\mathbf{u}}(\xi = 0) = \mathbf{0}, \quad (16)$$

where

$$\mathbf{K}_0 = \int_\eta \mathbf{B}_\xi^\text{T}(\eta) \mathbf{E} \mathbf{B}_\xi(\eta) \det(\mathbf{J}_\eta) \, d\eta, \quad \mathbf{S}_\xi = \int_\eta \mathbf{B}_\xi^\text{T}(\eta) \mathbf{E} \mathbf{S} \det(\mathbf{J}_\eta) \, d\eta,$$

$$\mathbf{K}_1 = \int_\eta \mathbf{B}_\eta^\text{T}(\eta) \mathbf{E} \mathbf{B}_\xi(\eta) \det(\mathbf{J}_\eta) \, d\eta, \quad \mathbf{S}_\eta = \int_\eta \mathbf{B}_\eta^\text{T}(\eta) \mathbf{E} \mathbf{S} \det(\mathbf{J}_\eta) \, d\eta,$$

$$\mathbf{K}_2 = \int_\eta \mathbf{B}_\eta^\text{T}(\eta) \mathbf{E} \mathbf{B}_\eta(\eta) \det(\mathbf{J}_\eta) \, d\eta.$$

\mathbf{E} denotes the stiffness matrix of the orthotropic Hooke's Law transformed into the global laminate coordinate system. Eq. (14) represents a second order, linear, non-homogeneous, ordinary differential equation system with variable coefficients. The homogeneous part of the equation has a certain structure (Euler-Cauchy-equation) and can be reduced to equations with constant coefficients by introducing the substitution $t = \ln(\xi)$:

$$\mathbf{K}_0 \hat{\mathbf{u}}_{,tt}(t) + (\mathbf{K}_1^\text{T} - \mathbf{K}_1) \hat{\mathbf{u}}_{,t}(t) - \mathbf{K}_2 \hat{\mathbf{u}}(t) = \mathbf{0}. \quad (17)$$

Furthermore, the second order differential equations (17) are transformed into first order equations using $\hat{\mathbf{v}}(t) = \frac{\partial \hat{\mathbf{u}}}{\partial t}$

$$\begin{bmatrix} \hat{\mathbf{v}}_{,t} \\ \hat{\mathbf{u}}_{,t} \end{bmatrix} = \underbrace{\begin{bmatrix} -\mathbf{K}_0^{-1} (\mathbf{K}_1^\text{T} - \mathbf{K}_1) & \mathbf{K}_0^{-1} \mathbf{K}_2 \\ \mathbf{I} & \mathbf{0} \end{bmatrix}}_{\boldsymbol{\kappa}} \begin{bmatrix} \hat{\mathbf{v}} \\ \hat{\mathbf{u}} \end{bmatrix}. \quad (18)$$

Incorporating the exponential approach

$$\begin{bmatrix} \hat{\mathbf{v}} \\ \hat{\mathbf{u}} \end{bmatrix} = e^{\lambda t} \begin{bmatrix} \boldsymbol{\Psi} \\ \boldsymbol{\Phi} \end{bmatrix} \quad (19)$$

into (18) yields the eigenvalue problem

$$(\boldsymbol{\kappa} - \lambda \mathbf{I}) \begin{bmatrix} \boldsymbol{\Psi} \\ \boldsymbol{\Phi} \end{bmatrix} = \mathbf{0}, \quad (20)$$

which is solved numerically using the QR-algorithm. It can be shown that the eigenvalue spectrum must be symmetric with respect to zero. Six zero eigenvalues are obtained representing

deformation modes due to rigid body motions as well as single forces. Only three corresponding linearly independent eigenvectors are obtained. These eigenvectors are related to rigid body motions. Hence, the missing eigenvectors have to be determined in order to obtain a fundamental solution. Since there do not exist single forces in the present problem, the determination of the corresponding eigenvectors is not further pursued. Using the back substitution the reduced homogeneous solution is given by

$$\hat{\mathbf{u}}(\xi) = \sum_{i=1}^{2n-3} c_i \xi^{\lambda_i} \Phi_i = \mathbf{c} \mathbf{D}(\xi) \Phi_{\mathbf{u}}, \quad (21)$$

where the single force modes are not considered and n denotes the length of the vector $\hat{\mathbf{u}}$. The particular solution of the non-homogeneous differential equations can be found by the method of undetermined coefficients. Hence, the approach

$$\hat{\mathbf{u}}_{\mathbf{p}} = \Phi_{\mathbf{p}} \xi, \quad (22)$$

is incorporated into Eq. (14) yielding a system of linear equations with respect to $\Phi_{\mathbf{p}}$

$$(\mathbf{K}_0 + \mathbf{K}_1^T - \mathbf{K}_1 - \mathbf{K}_2) \Phi_{\mathbf{p}} = \mathbf{S}_{\eta} - \mathbf{S}_{\xi}, \quad (23)$$

The total displacement is finally given by

$$\hat{\mathbf{u}}(\xi) = \mathbf{c} \mathbf{D}(\xi) \Phi_{\mathbf{u}} + \Phi_{\mathbf{p}} \xi. \quad (24)$$

Subsequently, the unknown constants \mathbf{c} are determined by substituting Eq. (24) into Eq. (15) and Eq. (16). It is worth to mention that Eq. (16) can only be fulfilled if the constants corresponding to eigenvalues $\lambda_i < 0$ become zero. Hence, only deformation modes with $\lambda_i \geq 0$ are considered. In conclusion, the sought displacements $\hat{\mathbf{u}}(\xi, \eta)$ are given by Eq. (12).

In the following the results obtained by the SBFEM using linear shape functions are introduced. Initially, the singular character of the stress field with respect to the laminate layup is discussed. The SBFEM can be advantageously applied to singular stress fields due to the fact that the solution of the eigenvalue problem (20) yields the corresponding singularity order. As shown in Figure 5, the free-edge effect induces weak stress singularities.

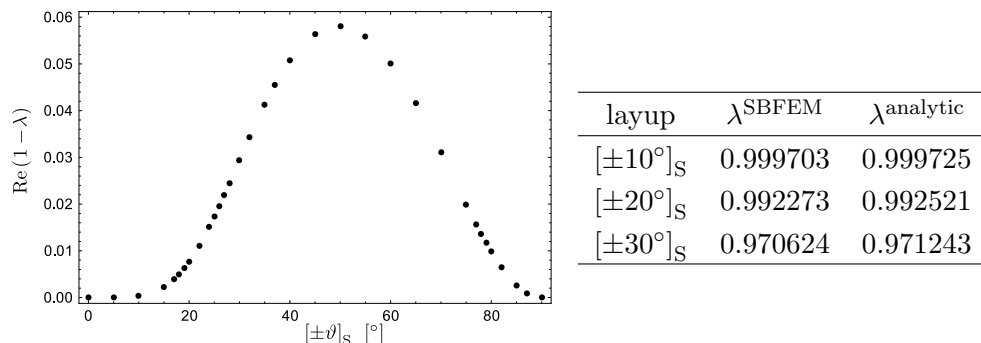


Figure 5: *Left*: Examination of singular eigenvalues ($0 < \lambda < 1$) for selected G947/M18 angle-ply laminates by means of the SBFEM (195 degrees of freedom). *Right*: In comparison, singular eigenvalues predicted numerically, and analytically. Even with a few degrees of freedom, the singularity order predicted by the SBFEM is reproduced very accurately.

The singularity order $\text{Re}(1 - \lambda)$ strongly depends on the laminate layup. A growing ply angle ϑ goes along with an increasing singularity order up to $\vartheta = 45^\circ$, where the effect becomes maximum. Based on the results shown in Figure 3, it can be concluded that an increasing singularity order goes along with a reduction of the effective laminate strength in the sense of interlaminar crack onset.

Solving the boundary value problem yields the sought displacement field. As depicted in Figure 6 the in-plane deformation of the contour close to the free edge determined by SBFEM is in good agreement with the FEM reference solution. Hence, a good agreement for the application of the coupled criterion compared to the FE reference solution can be expected. An assessment based on the SBFEM stress solution is subject of current research.

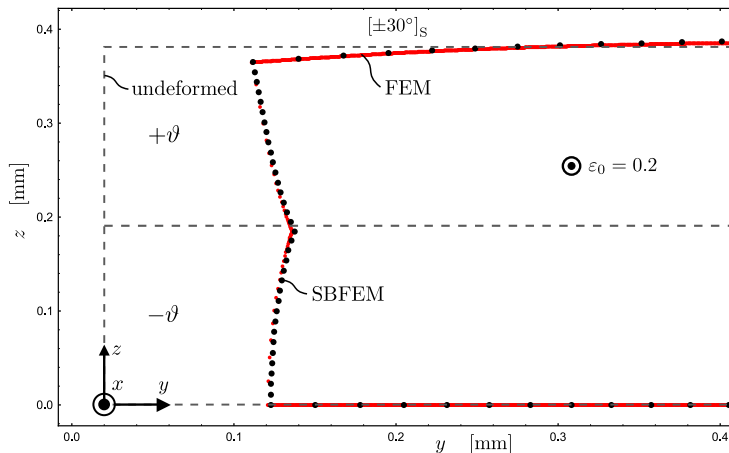


Figure 6: Deformed contour of the quarter model determined by FEM (red marked) as well as SBFEM for an G947/M18 angle-ply laminate ($b = 0.57$ mm).

7 Conclusion

The finite fracture mechanics approach has been applied to the free-edge effect in composite laminates in order to predict interface crack onset. First, the required stresses and incremental energy release rates have been obtained by means of the finite element method. Good results have been achieved compared to experiments from literature. Subsequently, the scaled boundary finite element method has been implemented in order to reduce the computational effort. Results show the high potential of the scaled boundary finite element method compared to the finite element method regarding the numerical effort and accuracy. The displacements obtained by the SBFEM are in good agreement with the FEM solution. As a next step, the quantities determined by the SBFEM will be used for developing an efficient FFM failure model for interface crack onset in composite laminates.

8 Acknowledgment

The authors highly appreciate the financial support of the German Research Foundation (DFG) under grant No BE1090/44-1.

REFERENCES

- [1] Hayashi, T.: Analytical Study of Interlaminar Shear Stresses in Laminated Composite Plate. *Space Technology and Science: Proc. of the seventh international symposium* (1967), Tokyo.
- [2] Pipes, R.B. and Pagano, N.J.: Interlaminar Stresses in Composite Laminates Under Uniform Axial Extension. *Journal of Composite Materials* (1970) **4**, pp. 538–548.
- [3] Kant, T. and Swaminathan, K.: Estimation of transverse/interlaminar stresses in laminated composites - a selective review and survey of current developments. *Composite Structures* (2000) **49**, pp. 65–75.
- [4] Mittelstedt, C. and Becker, W.: Interlaminar Stress Concentrations in Layered Structures: Part I - a Selective Literature Survey on the Free-Edge Effect since 1967. *Journal of Composite Materials* (2004) **38**, pp. 1037–1061.
- [5] Whitney, J.M.; Nuismer, R.J.: Stress Fracture Criteria for Laminated Composites Containing Stress Concentrations. *Journal of Composite Materials* (1974) **8**, pp. 253–265.
- [6] O'Brien, T.K.: Characterization of Delamination Onset and Growth in a Composite Laminate. ASTM STP 775 (1982), pp. 140–167.
- [7] Leguillon, D.: A method based on singularity theory to predict edge delamination of laminates. *International Journal of Fracture* (1999) **100(1)**, pp. 105–120.
- [8] Awerbuch, J.; Madhukar, M.S.: Notched Strength of Composite Laminates: Predictions and Experiments - A Review. *Journal of Reinforced Plastics and Composites* (1985) **4**, pp. 1–157.
- [9] Pipes, R.B.; Wetherhold, R.C.; Gillespie, J.W.: Notched Strength of Composite Materials. *Journal of Composite Materials* (1979) **13**, pp. 148–160.
- [10] Tan, S.C.: Fracture strength of composite laminates with an elliptical opening. *Composites Science and Technology* (1987) **29(2)**, pp. 133–152.
- [11] Leguillon, D.: Strength or toughness? A criterion for crack onset at a notch. *European Journal of Mechanics-A/Solids* (2002) **21(1)**, pp. 61–72.
- [12] Weissgraeber, P.; Leguillon, D.; Becker, W.: A review of Finite Fracture Mechanics: crack initiation at singular and non-singular stress raisers. *Archive of Applied Mechanics* (2016) **86(1-2)**, pp. 375–401.
- [13] Martin, E.; Leguillon, D.; Carrere, N.: A twofold strength and toughness criterion for the onset of free-edge shear delamination in angle-ply laminates. *International Journal of Solids and Structures* (2010) **47**, pp. 1297–1305.
- [14] Lagunegrand, L.; Lorriot, T.; Harry, R.; Wargnier, H.; Quenisset, J.M.: Initiation of free-edge delamination in composite laminates. *Composites Science and Technology*. (2006) **66**, pp. 1315–1327.
- [15] Song, C. and Wolf, J.: Consistent Infinitesimal Finite-Element-Cell Method: Out-of-Plane Motion. *Journal of Engineering Mechanics* (1995) **121(5)**, pp. 613–619.
- [16] Sun, Z.; Ooi, E.T.; Song, C.: Finite fracture mechanics analysis using the scaled boundary finite element method. *Engineering Fracture Mechanics* (2015) **134**, pp. 330–353.
- [17] Hexcel Cooperation, HexPly M18, datasheet, 2016.
- [18] Bradley, W.L.: Relationship of matrix toughness to interlaminar fracture toughness. In Friedrich, K. (Ed.) *Application of fracture mechanics to composite materials*, Elsevier, Amsterdam, 1989.
- [19] Pereira, A.B. and de Morais, A.B.: Mode I interlaminar fracture of carbon/epoxy multidirectional laminates. *Composites Science and Technology* (2004) **64**, pp. 2261–2270.